

Realization of electron-deficient Ru sites via Co₄N coupling for synergistically enhanced alkaline hydrogen evolution

Mengyuan Xing^{a†}, Xuyun Guo^{c†}, Wenfang Yuan^a, Wenxuan Chen^a, Mengmeng Du^a, Lejuan Cai^{*b}, Valeria Nicolosi^c, Yang Chai^d, and Bocheng Qiu^{*a}

Materials: Nickel foam (NF) was purchased from Lizhiyuan Technology Co., Ltd. (Taiyuan, China). Urea ($\text{CO}(\text{NH}_2)_2$, $\geq 99.0\%$) was purchased from Xilong Scientific Co., Ltd. (Guangdong, China). Ammonium fluoride (NH_4F , $\geq 96.0\%$) and anhydrous ethanol ($\text{C}_2\text{H}_5\text{OH}$, $\geq 99.7\%$) were purchased from Sinopharm Chemical Reagent Co. Ltd. (Shanghai, China). Cobalt nitrate hexahydrate ($\text{Co}(\text{NO}_3)_2 \cdot 6\text{H}_2\text{O}$, 99%) and Ruthenium (III) chloride hydrate ($\text{RuCl}_3 \cdot 3\text{H}_2\text{O}$, 98%) were purchased from Macklin Biochemical Co., Ltd. Potassium hydroxide (KOH, 95%) and Pt/C (5 wt% Pt) were purchased from Shanghai Aladdin Bio-Chem Technology Co., Ltd.

Preparation of Ru/Co₄N/NF: Nickel foam substrate (NF, 2.5×3.5 cm) was pretreated with 3 M HCl to remove the oxide layer and impurity on the surface, and then washed by distilled (DI) water and ethanol for several times. The cleaned NF was immersed in the mixed solution containing 28 mM $\text{Co}(\text{NO}_3)_3 \cdot 6\text{H}_2\text{O}$, 140 mM $\text{CO}(\text{NH}_2)_2$, and 111 mM NH_4F , which was then transferred into a 50 mL Teflon-lined autoclave and kept at 100 °C for 10 h to obtain Co(OH)F/NF. The as-made Co(OH)F/NF was subsequently soaked in 0.2 mg mL⁻¹ of RuCl_3 ethanol solution for 30 min, and then washed by DI water and dried in an oven. Finally, Ru/Co₄N/NF was fabricated by nitridation of the prepared Co(OH)F/NF in a tube furnace system at 500 °C for 2h under the NH_3/N_2 (15 vol%/85 vol%) atmosphere, and the molar ratio of Ru to Co is determined to be approximately 1/10.6 using inductively coupled plasma mass spectrometry (ICP-MS). Ru/Co₄N/NF with different Ru/Co molar ratios of 1:14.2, 1:7.4, and 1:5.7 were obtained by immersing into the RuCl_3 alcohol solution with 0.1 mg mL⁻¹, 0.3 mg mL⁻¹, and 0.4 mg mL⁻¹ for 30 min, respectively. For comparison, Co₄N/NF was also synthesized by the calcination of Co(OH)F/NF at 500 °C for 2h under the NH_3/N_2 atmosphere. Ru/NF was obtained by soaking the pretreated nickel foam in a solution of 0.2 mg mL⁻¹ RuCl_3 alcohol for 30 min directly and calcined at 500°C for 2 h under the NH_3/N_2 atmosphere.

Material characterizations: The morphologies of all the samples were observed using scanning electron microscope (SEM; Hitachi S4800), transmission electron microscope (TEM; JEOL1400), and high-resolution transmission electron microscope (HRTEM; JEOL 2100F). The element mapping was recorded by energy-dispersive X-ray spectroscopy (EDX) attached to the JEOL 2100F. X-ray photoelectron spectroscopy (XPS, Perkin-Elmer PHI 5000C ESCA system) was collected under Al K α radiation operated at 250 W. The crystal structures of all the catalysts were examined using powder X-ray diffractometer with Cu K α radiation ($\lambda = 1.5406 \text{ \AA}$) in the range from 10° to 80° (2 θ).

Electrochemical Measurements: The electrochemical activities were tested on a CHI 660E electrochemical station with a three-electrode configuration in 1.0 M KOH at room temperature. The loading densities of all the catalysts are controlled to be 1.0 mg

cm⁻² using ultrasonic treatment. The Ru/Co₄N/NF (0.5 × 0.5 cm) were used as the working electrode with a carbon rod and a standard Hg/HgO electrode as the counter electrode and the reference electrode, respectively. The Pt/C electrode was prepared via the following method: 2 mg of commercial Pt/C (Pt 5 wt%) was added into the mixed solvent containing 17 μL of Nafion, 117 μL of ethanol, and 533 μL of DI water, and 170 μL of the above suspension was dropped onto the NF substrate (0.5 * 0.5 cm). Note that the Pt loading density is approximately 50 μg cm⁻². The potentials applied in the LSV studies in 1.0 M KOH solution were calibrated with respect to RHE by the equation $E(\text{RHE}) = E(\text{Hg}/\text{HgO}) + 0.098 + 0.0592 \cdot \text{pH} = E(\text{Hg}/\text{HgO}) + 0.927$. All the potentials were corrected by eliminating the electrolyte resistances (*i.e.*, IR loss). The introduction of IR-corrected LSV curves makes up for the electrode potential loss at medium to high current region caused by the solution resistance. The compensated potential was corrected by the equation: $E_{\text{compensated}} = E_{\text{measured}} - i \cdot R_s$, where R_s was determined by the electrochemical workstation. HER polarization curves obtained from LSV was recorded at a scan rate of 5 mV s⁻¹ from -0.37 to 0.03 V vs. RHE. Electrochemical impedance spectra (EIS) were performed from 100 kHz to 0.01 Hz at -0.07 V vs. RHE. The chronopotentiometry tests were conducted at constant current densities of 50 and 200 mA cm⁻². The stability test was further confirmed by cyclic voltammetry (CV) sweeps from -0.2 to 0 V vs RHE at a scan rate of 50 mV s⁻¹ for 1000 cycles. CV method was used to measure the electrochemical double layer capacitance (C_{dl}), and the potential was swept at different scan rates of 5, 10, 15, 20, and 25 mV s⁻¹ from 0.78 to 0.88 V vs. RHE. The C_{dl} value was calculated using the following equation: $C_{\text{dl}} = (j_a - j_c) / 2v$, where j_a , j_c , and v were the anodic current density (mA cm⁻²), the cathodic current density (mA cm⁻²), and the scan rate (mV s⁻¹), respectively. Electrochemical surface area (ECSA) was calculated by the equation: $\text{ECSA} = C_{\text{dl}}/C_s$, where C_s is the double layer capacitance of an ideally flat electrode, which is usually taken as 40 μF cm⁻² in an alkaline electrolyte.¹

DFT calculations: The Vienna Ab initio Simulation Package was employed to perform density functional calculations, with the Perdew, Burke, and Ernzerhof (PBE) functional to describe the exchange-correlation interactions and the projector augmented-wave method to represent the core-valence electron interactions.^{2, 3} The energy cutoff was set to 520 eV, and convergence criteria were established as 10⁻⁴ eV/atom for energy and 0.01 eV Å⁻¹ for force, respectively. Initially, a pristine (3 × 3) Co₄N (100) slab was optimized, and then it was combined with a Ru₁₉ cluster to construct the Ru/Co₄N structure. It is important to note that the structures of the Co₄N substrate and Ru₁₉ cluster were also considered as the control samples in this study. The adsorption energies of H₂O and H* on Co₄N, Ru₁₉, and Ru/Co₄N substrates were calculated using the formula of $\Delta G = G_2 - (G_1 + E_{\text{sub}})$, where G_2 is the Gibbs energy of the Co₄N substrate with adsorbed H₂O or H*, G_1 is the Gibbs energy of the H₂O or H*, and E_{sub} is the energy of the Co₄N substrate. The zero-point energy and entropy corrections under the standard conditions ($p_0 = 1$ bar and $T_0 = 298.15$ K) were considered, and the chemical potential of proton and electron was described based on

the computational hydrogen electrode.^{4, 5} To realize a better description of the interactions between the adsorbates and substrates, the vdw-DF2 method was applied to describe the van der Waals interactions in our models.^{6, 7} The vacuum layer was set as 20 Å to avoid spurious interaction between adjacent slabs. The Brillouin zone was sampled using Monkhorst–Pack meshes of $3 \times 3 \times 1$ for the structure optimizations and $5 \times 5 \times 1$ for the static calculations.

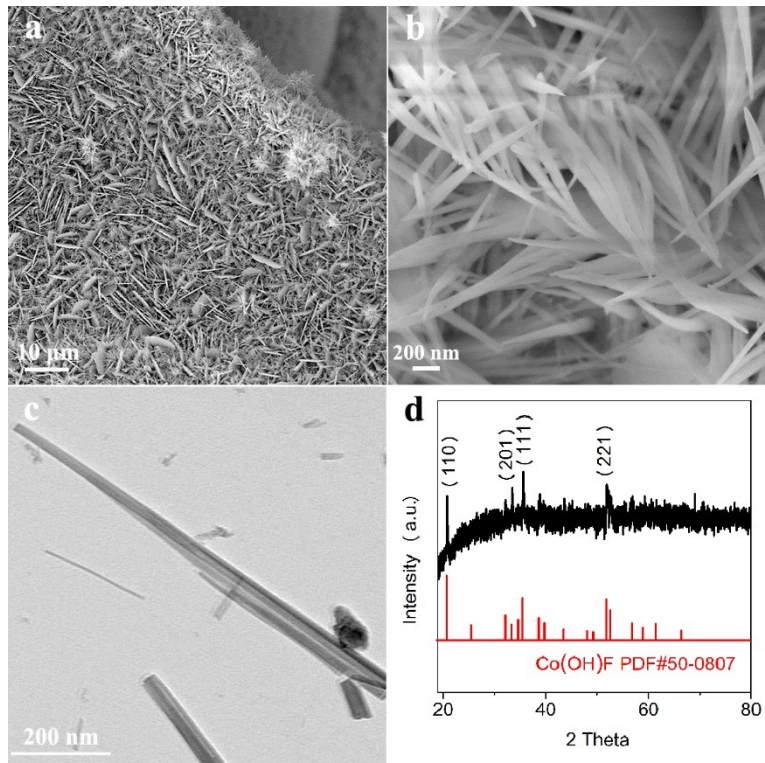


Fig. S1 (a-b) SEM images, (c) TEM image, and (d) XRD pattern of Co(OH)F/NF.

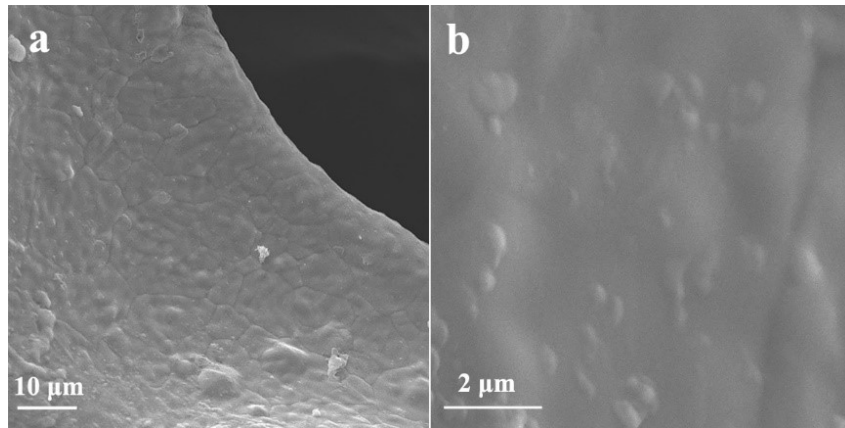


Fig. S2 (a-b) SEM images of pristine NF.

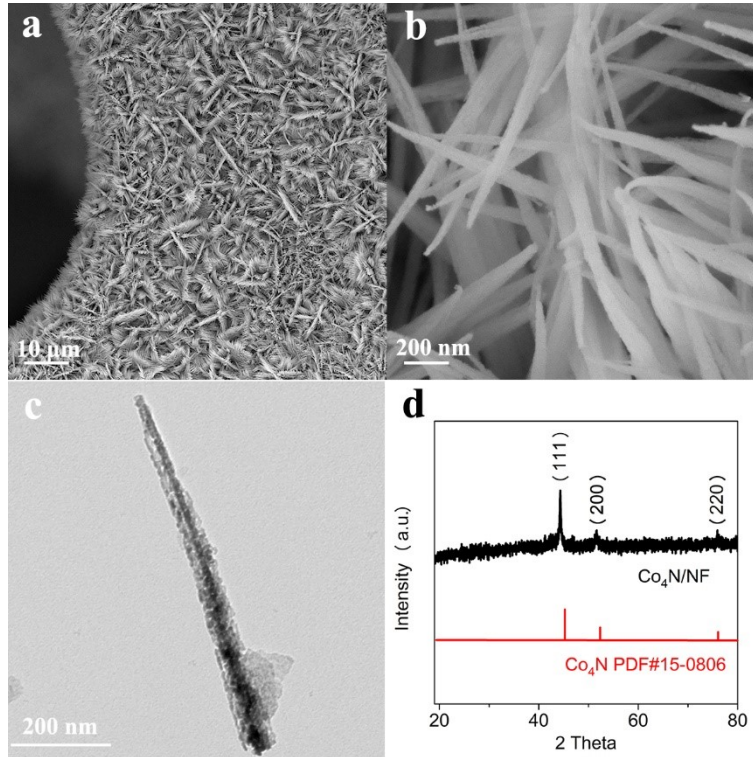


Fig. S3 (a-b) SEM images, (c) TEM image, and (d) XRD pattern of $\text{Co}_4\text{N}/\text{NF}$.

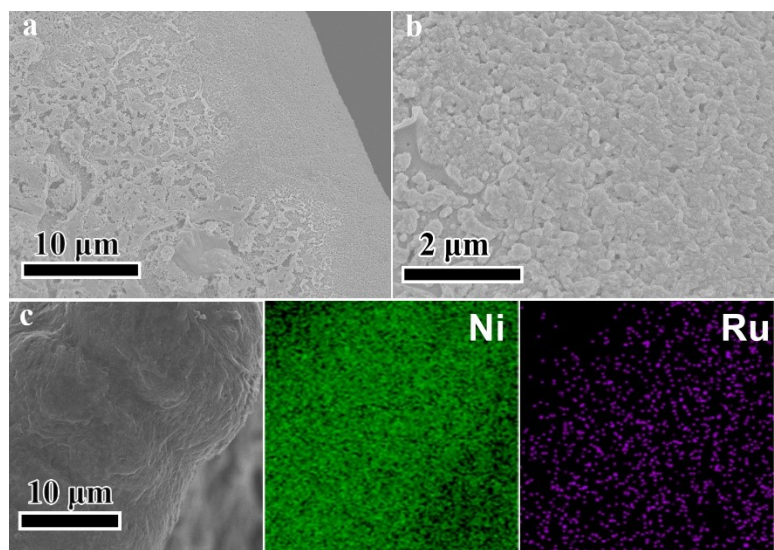


Fig. S4 (a-b) SEM images of Ru/NF and (c) the corresponding element mapping.

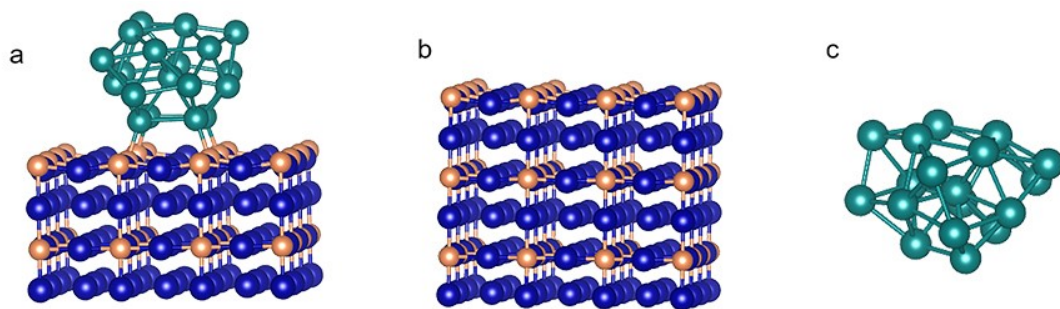


Fig. S5 The constructed theoretical models of Ru/Co₄N (a), Co₄N (b), and Ru (c).

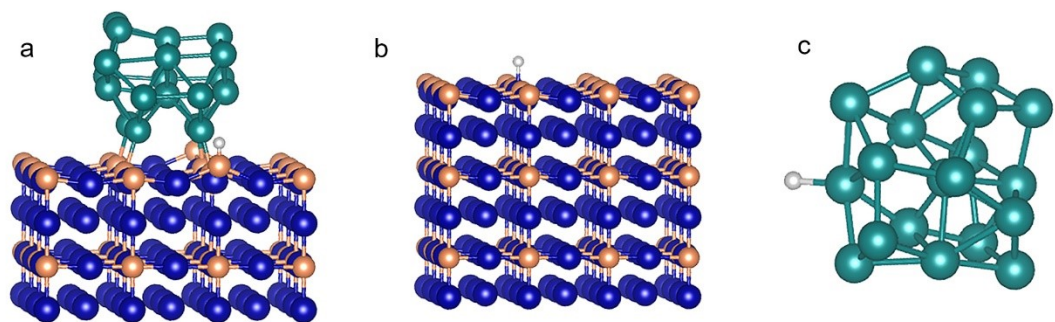


Fig. S6 The calculated theoretical models with the adsorbed H over Ru/Co₄N (a), Co₄N (b), and Ru (c).

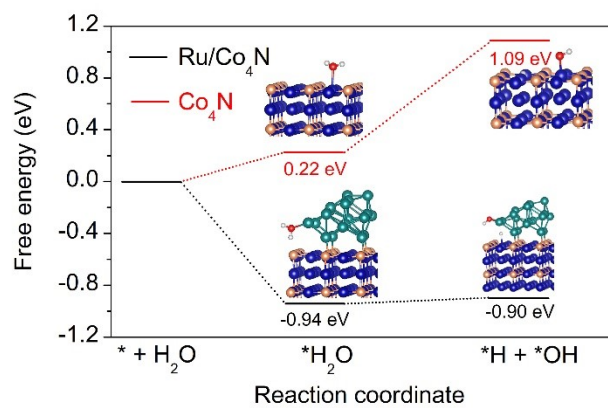


Fig. S7 The calculated free energy of water dissociation over Ru/Co₄N and Co₄N.

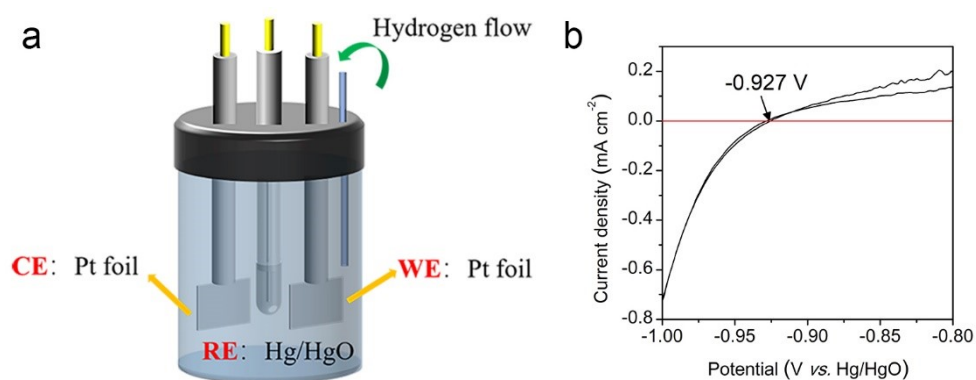


Fig. S8 (a) Experimental setup for the three-electrode cell for the reference electrode (RE, Hg/HgO) calibration. Pt foils were utilized as both counter electrode (CE) and working electrode, and the electrolyte (1 M KOH) was saturated by high-purity H₂. (b) Linear sweep voltammetry (LSV) curve of the Hg/HgO electrode calibration in 1 M KOH recorded at a scan rate of 1 mV s⁻¹ at room temperature. The average of the two interconversion point values was taken as the thermodynamic potential, namely -0.927 V. Therefore, the potential value can be calculated by the following equation: $E(\text{RHE}) = E(\text{Hg}/\text{HgO}) + 0.927$.

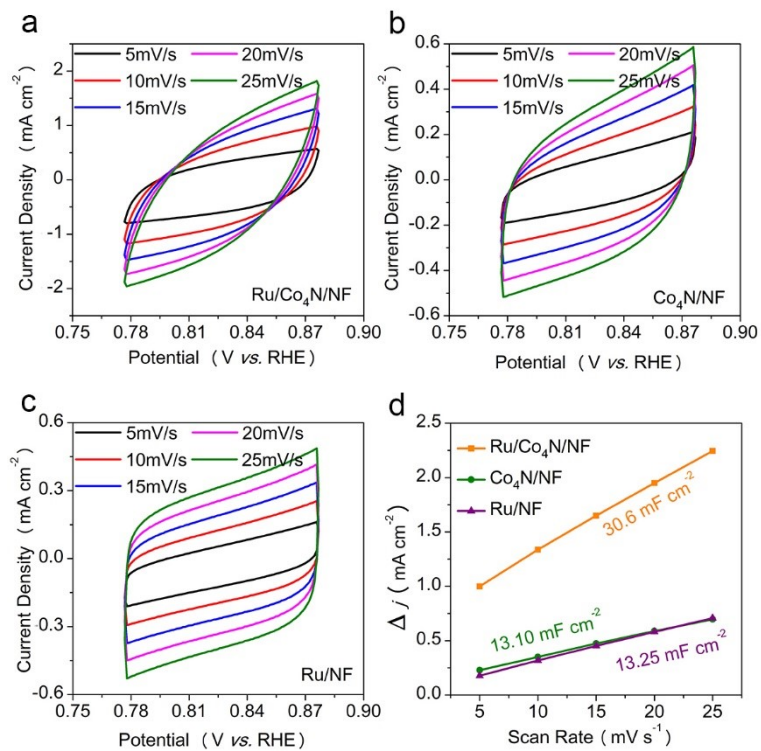


Fig. S9 Cyclic voltammetry curves for (a) Ru/Co₄N/NF, (b) Co₄N/NF, and (c) Ru/NF in the non-Faradaic capacitive range at the scanning rate of 5, 10, 15, 20, and 25 mV s⁻¹. (d) The corresponding plots of Δj ($\Delta j = j_a - j_c$, j_a and j_c were recorded at 0.85 V vs. RHE) as a function of scan rates.

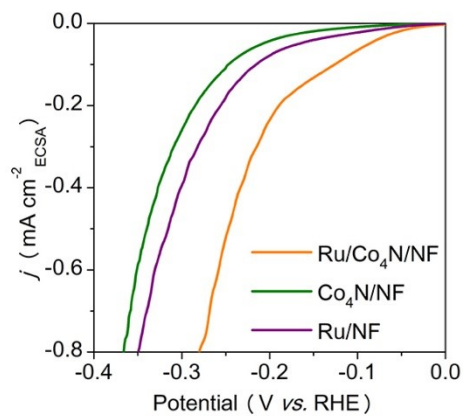


Fig. S10 Polarization curves of various catalysts normalized by their corresponding ECSA values.

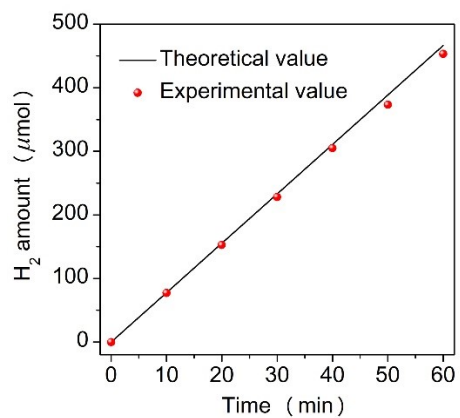


Fig. S11 The theoretically calculated and experimentally measured hydrogen amount as a function of time for HER over Ru/Co₄N/NF at a current density of 50 mA cm⁻² in 1.0 M KOH.

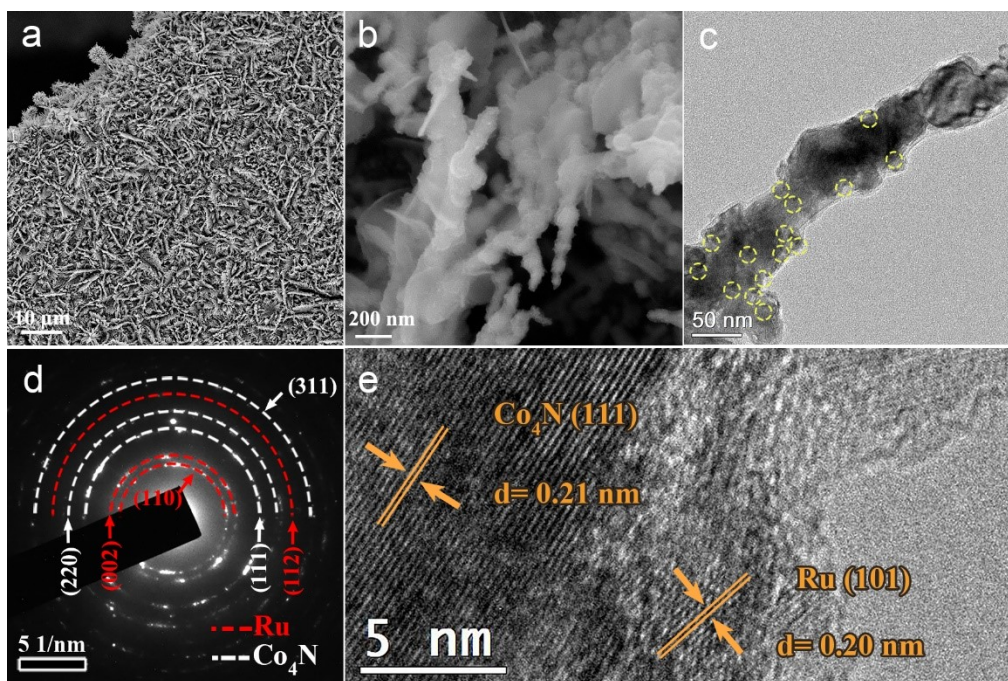


Fig. S12 (a-b) SEM images, (c) TEM image, (d) The SAED pattern, and (e) HRTEM image of the recovered Ru/Co₄N/NF catalysts after 50 h chronopotentiometry measurement at 50 mA cm⁻².

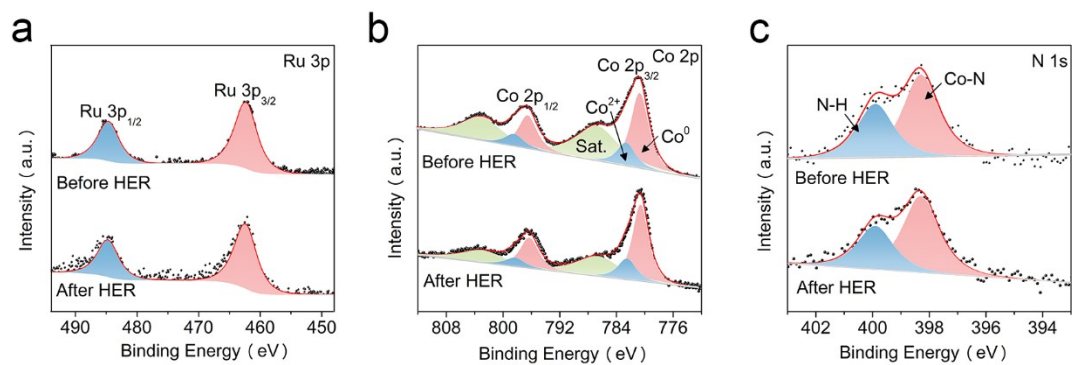


Fig. S13 XPS spectra of (a) Ru 3p, (b) Co 2p, and (c) N 1s for Ru/Co₄N/NF before and after 50 h chronopotentiometry measurement.

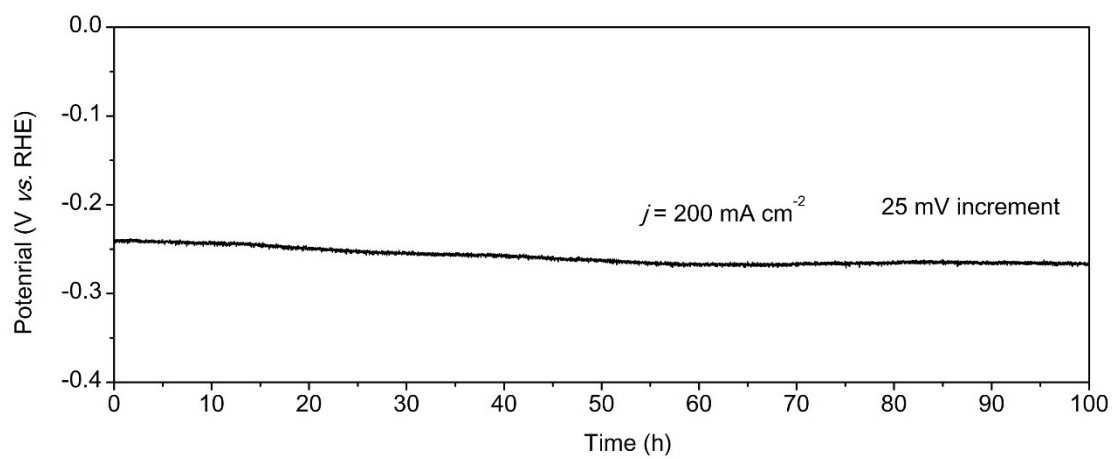


Fig. S14 Chronopotentiometry measurement of Ru/Co₄N/NF at the current density of 200 mA cm⁻².

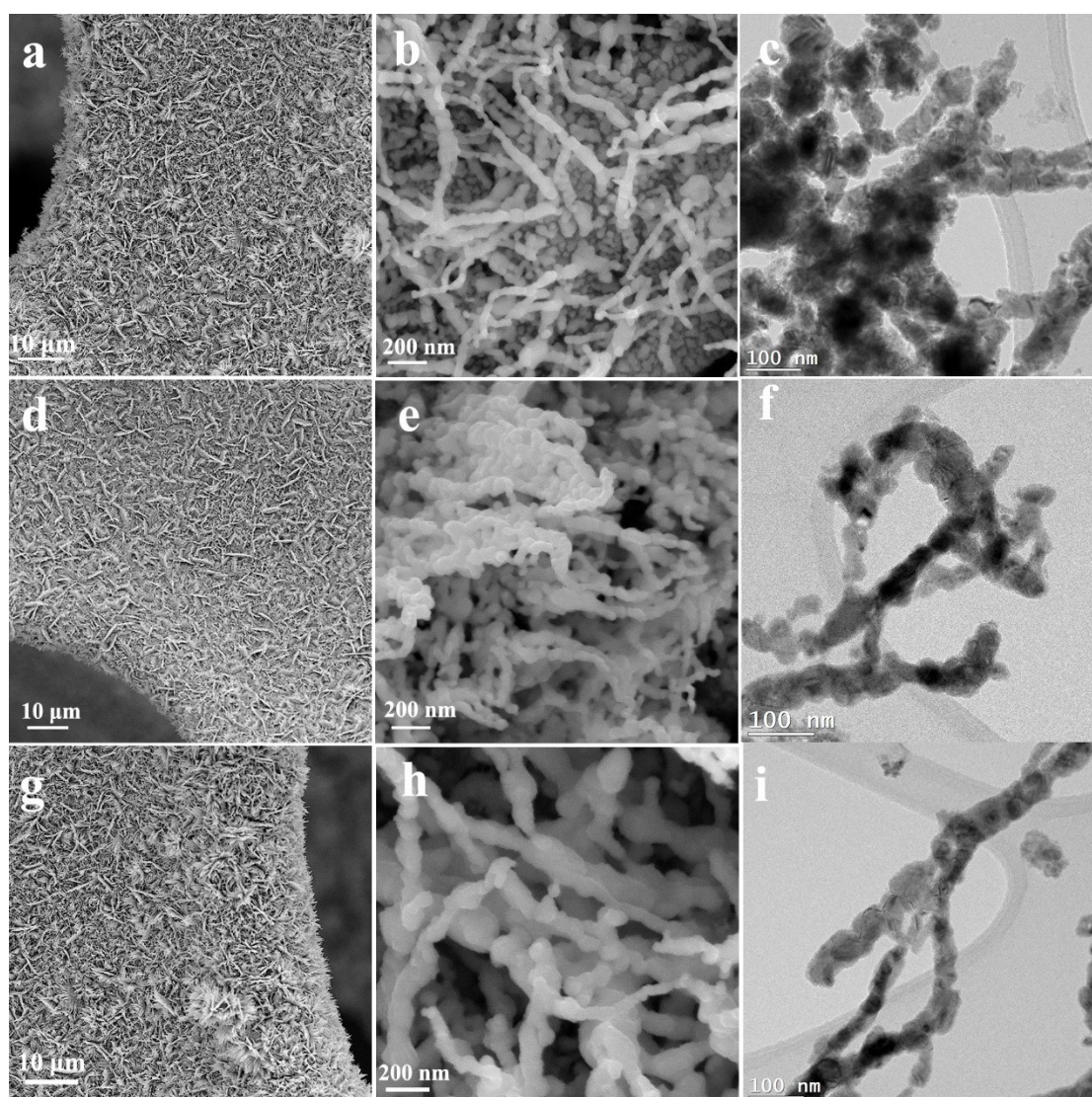


Fig. S15 (a-b) SEM images and (c) HRTEM images of Ru/Co₄N/NF with the Ru/Co molar ratio of 1:14.2, (d-e) SEM images and (f) HRTEM images of with the Ru/Co molar ratio of 1:7.4, (g-h) SEM images and (i) HRTEM images of with the Ru/Co molar ratio of 1:5.7.

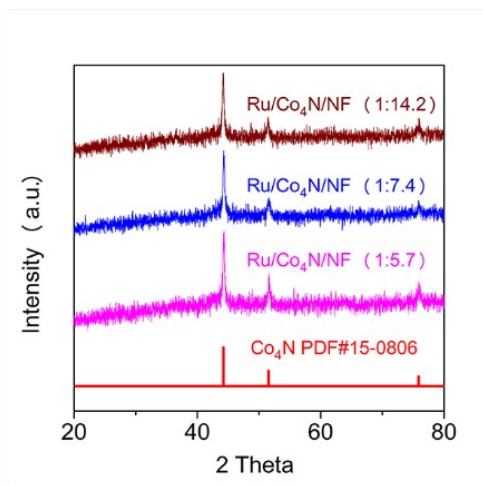


Fig. S16 XRD patterns of Ru/Co₄N/NF with various molar ratios of Ru to Co.

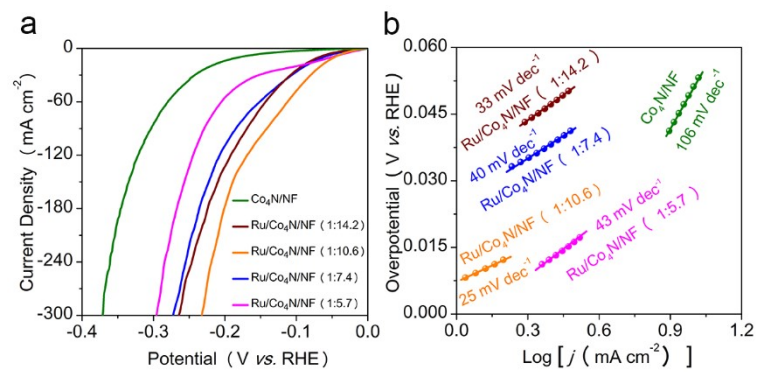


Fig. S17 (a) Polarization curves and (b) Tafel slopes of Co₄N/NF and Ru/Co₄N/NF with various molar ratios of Ru to Co.

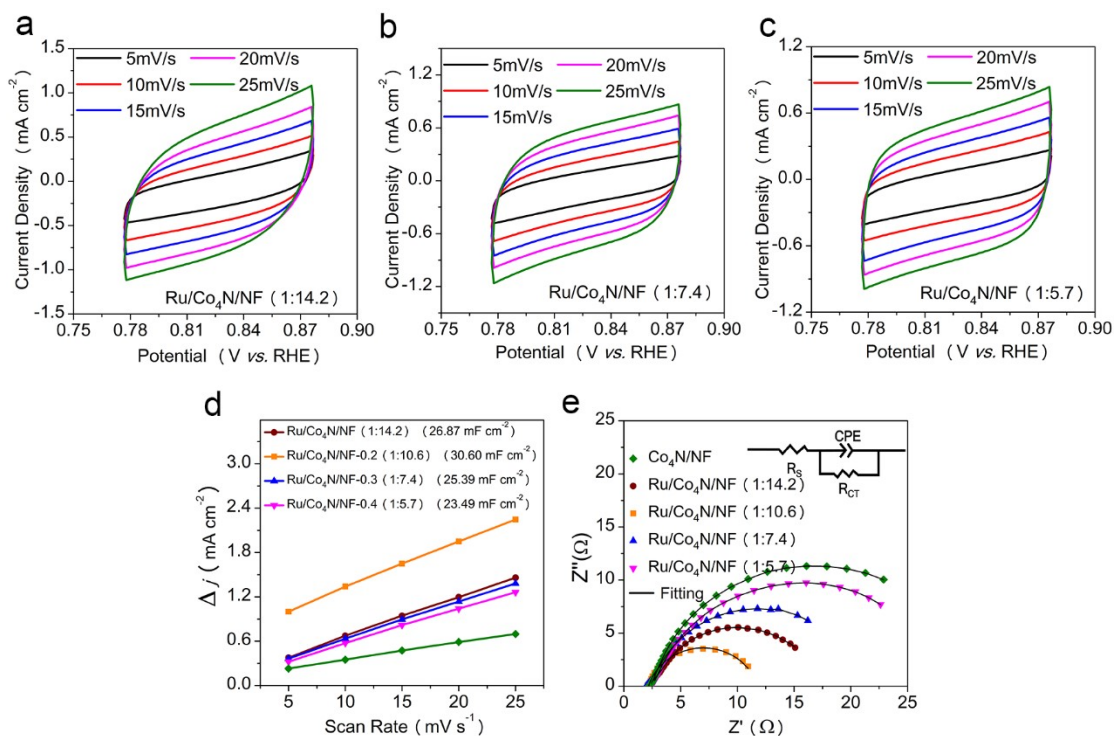


Fig. S18 (a-c) CV curves of various electrodes in the double layer capacitive region at the scan rate of 5~25 mV s⁻¹. (d) Capacitive currents as a function of scan rates for Co₄N/NF and Ru/Co₄N/NF. Note that $\Delta j = j_a - j_c$, where j_a and j_c were recorded at 0.82 V vs RHE. (e) Electrochemical impedance spectra (EIS) of Co₄N/NF and Ru-Co₄N/NF measured at the overpotential of 70 mV, and the inset is the equivalent circuit mode.

Table S1. The as-prepared Ru/Co₄N/NF with the various molar ratios of Ru to Co.

Catalysts	RuCl ₃ /ethanol solution with different concentrations	The measured ratio of Ru to Co determined by ICP-MS
Ru/Co ₄ N/NF	0.1 mg ml ⁻¹	1: 14.2
	0.2 mg ml ⁻¹	1: 10.6
	0.3 mg ml ⁻¹	1: 7.4
	0.4 mg ml ⁻¹	1: 5.7

Table S2 Comparison of HER performance for Ru/Co₄N/NF with the ever-reported metal nitrides in alkaline condition (1 M KOH). *n.a.* indicates not available.

Catalyst	$\eta_{10/100}$ (mV)	Tafel slope (mV dec ⁻¹)	Ref.
Ru/Co ₄ N/NF	45/145	25	This work
Ru/Ni ₃ N-Ni	53/135	32	8
Ru-NiWN _x /NF	28/70	33	9
cRu-Ni ₃ N/NF	32/99	26	10
Ru-Ni ₃ N@NC	43/120	70	11
Ru NRs/TiN	25/150	27	12
Ru-VN	144/ <i>n.a.</i>	73	13
Ru-Ni ₃ N	51/119	55	14
Cr-Co ₄ N NR/CC	21/99	38	15
V-Co ₄ N	37/ <i>n.a.</i>	41	16
NiCoN/C	137/173	69	17
Co ₃ FeN _x	23/147	94	18
NiCoN/CC	68/180	69	19
NiCo ₂ N/NF	150/290	79	20
Co ₃ N	230/420	102	21
CoN _x /C	170/ <i>n.a.</i>	75	22
Co-Ni ₃ N	194/280	57	23
Ni ₃ N-NiMoN	31/220	64	24
Ni/Co ₂ N	16/140	61	25
V-Ni ₃ N/Ni	44/210	52	26
FeNi ₃ N	75/210	98	27
TiN@Ni ₃ N	21/70	42	28
CN _x @Ru/MW-CNTs	39/90	28	29

Table S3 The ECSA values of the various catalysts.

Catalysts	Co ₄ N/NF	Ru/NF	Ru/Co ₄ N/NF (Ru/Co=1:14.2)	Ru/Co ₄ N/NF (Ru/Co=1:10.6)	Ru/Co ₄ N/NF (Ru/Co=1:7.4)	Ru/Co ₄ N/NF (Ru/Co=1:5.7)
ECSA	331.3	460.5	671.8	765.0	589.8	587.3

Table S4 The fitted results of the EIS plots.

Catalysts	Co ₄ N/NF	Ru/NF	Ru/Co ₄ N/NF (Ru/Co=1:14.2)	Ru/Co ₄ N/NF (Ru/Co=1:10.6)	Ru/Co ₄ N/NF (Ru/Co=1:7.4)	Ru/Co ₄ N/NF (Ru/Co=1:5.7)
R _s (Ω)	2.6	2.6	2.6	2.6	2.6	2.6
R _{CT} (Ω)	28.2	26.2	14.7	7.2	18.8	25.2

References

1. B. Qiu, Y. Zhang, X. Guo, Y. Ma, M. Du, J. Fan, Y. Zhu, Z. Zeng and Y. Chai, *J. Mater. Chem. A*, 2022, **10**, 719-725.
2. J. P. Perdew, K. Burke and M. Ernzerhof, *Phys. Rev. Lett.*, 1996, **77**, 3865.
3. T. Bucko, J. Hafner, S. Lebègue and J. G. Angyán, *J. Phys. Chem. A*, 2010, **114**, 11814-11824.
4. V. Wang, N. Xu, J.-C. Liu, G. Tang and W.-T. Geng, *Computer Physics Communications*, 2021, **267**, 108033.
5. J. K. Nørskov, J. Rossmeisl, A. Logadottir, L. Lindqvist, J. R. Kitchin, T. Bligaard and H. Jonsson, *J. Phys. Chem. B*, 2004, **108**, 17886-17892.
6. M. Dion, H. Rydberg, E. Schröder, D. C. Langreth and B. I. Lundqvist, *Phys. Rev. Lett.*, 2004, **92**, 246401.
7. K. Lee, É. D. Murray, L. Kong, B. I. Lundqvist and D. C. Langreth, *Phys. Rev. B*, 2010, **82**, 081101.
8. Z. Liu, M. Zha, Q. Wang, G. Hu and L. Feng, *Chem. Commun.*, 2020, **56**, 2352-2355.
9. H. Wang, X. Cheng and Y. Tong, *J. Colloid Inter. Sci.* 2023, **629**, 155-164.
10. J. Zhu, R. Lu, W. Shi, L. Gong, D. Chen, P. Wang, L. Chen, J. Wu, S. Mu and Y. Zhao, *Energy Environ. Mater.*, 2023, **6**, e12318.
11. Y. Liu, D. Zheng, Y. Zhao, P. Shen, Y. Du, W. Xiao, Y. Du, Y. Fu, Z. Wu and L. Wang, *Int. J. Hydrogen Energ.*, 2022, **47**, 25081-25089.
12. Y. Yang, D. Wu, R. Li, P. Rao, J. Li, P. Deng, J. Luo, W. Huang, Q. Chen and Z. Kang, *Appl. Catal. B: Environ.*, 2022, **317**, 121796.
13. W. Wang, Y. Shao, Z. Wang, Z. Yang, Z. Zhen, Z. Zhang, C. Mao, X. Guo and G. Li, *ChemElectroChem*, 2020, **7**, 1201-1206.
14. X. Gao, W. Zang, X. Li, Z. Wang, L. Zheng and Z. Kou, *Chem. Eng. J.*, 2023, **451**, 138698.
15. N. Yao, P. Li, Z. Zhou, Y. Zhao, G. Cheng, S. Chen and W. Luo, *Adv. Energy Mater.*, 2019, **9**, 1970159.

-
16. Z. Chen, Y. Song, J. Cai, X. Zheng, D. Han, Y. Wu, Y. Zang, S. Niu, Y. Liu and J. Zhu, *Angew. Chem. Int. Ed.*, 2018, **57**, 5076-5080.
 17. B. Geng, F. Yan, L. Liu, C. Zhu, B. Li and Y. Chen, *Chem. Eng. J.*, 2021, **406**, 126815.
 18. Y. Wang, D. Liu, Z. Liu, C. Xie, J. Huo and S. Wang, *Chem. Commun.*, 2016, **52**, 12614-12617.
 19. C. Ray, S. C. Lee, B. Jin, A. Kundu, J. H. Park and S. C. Jun, *J. Mater. Chem. A*, 2018, **6**, 4466-4476.
 20. Y. Wang, B. Zhang, W. Pan, H. Ma and J. Zhang, *ChemSusChem*, 2017, **10**, 4170-4177.
 21. Z. Xu, W. Li, Y. Yan, H. Wang, H. Zhu, M. Zhao, S. Yan and Z. Zou, *ACS Appl. Mater. Interfaces*, 2018, **10**, 22102-22109.
 22. H.-W. Liang, S. Brüller, R. Dong, J. Zhang, X. Feng and K. Müllen, *Nat. Commun.*, 2015, **6**, 7992.
 23. C. Zhu, A. L. Wang, W. Xiao, D. Chao, X. Zhang, N. H. Tiep, S. Chen, J. Kang, X. Wang and J. Ding, *Adv. Mater.*, 2018, **30**, 1705516.
 24. A. Wu, Y. Xie, H. Ma, C. Tian, Y. Gu, H. Yan, X. Zhang, G. Yang and H. Fu, *Nano Energy*, 2018, **44**, 353-363.
 25. K. Sun, T. Zhang, L. Tan, D. Zhou, Y. Qian, X. Gao, F. Song, H. Bian, Z. Lu and J. Dang, *ACS Appl. Mater. Interfaces*, 2020, **12**, 29357-29364.
 26. H. Zhang, J. Wang, F. Qin, H. Liu and C. Wang, *Nano Res.*, 2021, **14**, 3489-3496.
 27. B. Zhang, C. Xiao, S. Xie, J. Liang, X. Chen and Y. Tang, *Chem. Mater.*, 2016, **28**, 6934-6941.
 28. Q. Zhang, Y. Wang, Y. Wang, A. M. Al-Enizi, A. A. Elzatahry and G. Zheng, *J. Mater. Chem. A*, 2016, **4**, 5713-5718.
 29. W. Gou, J. Li, W. Gao, Z. Xia, S. Zhang and Y. Ma, *ChemCatChem*, 2019, **11**, 1970-1976.